Cold rolling behaviour of Cu with highly oriented nanotwins: the importance of local shear strain

IOP Conf. Series: Materials Science and Engineering **580** (2019) 012008 doi:10.1088/1757-899X/580/1/012008

Cold rolling behaviour of Cu with highly oriented nanotwins: the importance of local shear strain

Q H Lu, J S Bai, Z Cheng, L Lu

Shenyang National Laboratory for Materials Science, Institute of Metal Research, Chinese Academy of Sciences, Shenyang 110016, P. R. China

Email: LLu@imr.ac.cn

Abstract. To clarify the deformation mechanism of nanotwinned materials under a complex stress state and large strain level, the microstructure evolution of pure Cu samples with high density of preferentially oriented nanotwins cold rolled to a strain up to 65% was systematically characterized by means of electron backscatter diffraction and transmission electron microscopy in this study. Heterogeneous deformation behavior was observed in nanotwinned Cu at different rolling strains. At a rolling strain of 15%, uniform deformation carried by the interactions between dislocations and twin boundaries dominate. At the same time, a small amount of strain localization in the direction ±45 ° respective to the rolling direction takes place, carried by detwinning and shear bands. As the rolling strain increased to 50%, detwinning becomes a dominant deformation mechanism and produces a large amount of coarse twin/matrix lamellae. A unique laminated structure with high angle lamellar boundaries (larger than 50 ° misorientation angle) and an average lamellar thickness of about 150 nm evolves from the coarse twin/matrix lamellae. As the rolling strain is increased up to 65%, an extensive laminated structures embedded with a few preserved twin blocks are prevalently formed. It is found that the local shear strain plays a critical role in the microstructure evolution of the nanotwinned Cu under cold rolling. When the local shear strains are so small as to be negligible, uniform deformation is sustained by interactions of dislocation/twin boundaries and the nanoscale twins survive. As the local shear strain increases up to 1, detwinning prevails and results in coarse twin/matrix lamellae. When the local shear strain is larger than 1, formation of shear bands composed of dislocation cells, sub-grains and fragments of twin lamellae instead of the detwinning process takes place, finally evolving into a laminated structure.

1. Introduction

Nanotwinned (nt) metals have attracted extensive interest for their superior mechanical properties, such as high strength, considerable ductility and good work hardening [1-5]. The intrinsic deformation mechanisms of nt-metals under uniaxial deformation have been extensively investigated by experimental characterization [6-8], crystal plasticity modeling [9] and by molecular dynamics simulations [10-12]. It is well established that the plastic deformation of nt-metals is dominated by the interactions between dislocations and twin boundaries (TBs). The deformation behavior and the deformation mechanisms of nt-metals not only strongly depend on the inherent microstructural

parameters, such as twin length and twin thickness [13, 14], but also closely depend on the extrinsic deformation conditions, such as the strain rate [15, 16], temperature [6, 17], and loading direction [7].

For example, under uniaxial compression, the plastic deformation of nanotwin structures can be switched among three specific dislocation modes, namely, dislocations transferring across and piling up at twin boundaries (TBs) [18], dislocations gliding in-between the confined twin/matrix layers [3] and dislocation-mediated TBs migration (or detwinning) [19], only by changing the uniaxial loading orientation with respect to the twin plane [7]. Correspondingly, different dislocation-based deformation mechanisms result in quite different mechanical properties, including yield strength, ductility and work hardening [7].

Compared to uniaxial deformation, the plastic deformations of nt-metal under complex axial stress states, such as cold rolling [20], torsion [21], and nano-indentation [22] are much more complicated. Detwinning, the general deformation mechanism by coarsening of nanoscale twins, is predominantly observed under complex axial deformations [19, 21, 23-26]. Detwinning caused by the migration of TBs is driven by gliding of Shockley partials along TBs, which can be active from incoherent twin boundaries (ITBs) and twin steps on the coherent twin boundaries (CTBs) or nucleated from grain boundaries [19, 26, 27]. In-situ transmission electron microscopy (TEM) investigations have indicated that Shockley partial dislocations can be multiplied from CTBs via the dissociation of a perfect dislocation crossing a CTB under certain stress states, leading to the migration of CTBs [28]. Multiaxial stress states and high shear stresses under non-uniform deformation facilitate transmission of dislocations across TBs and promote the glide of Shockley partial dislocations along the TBs, enhancing the detwinning process in nt-metals.

In addition, the formation of shear bands due to severe local deformations also typically occurs in nt-metals deformed under high strain and complex stress conditions [29-32]. Hong et al. [26] studied the evolution of shear bands in Cu-Al under the dynamic plastic deformation (DPD) process and found that only when the activation of dislocations is heavily suppressed in the nanoscale twin structures, are shear bands nucleated from detwinning area, with further increase of the local shear strains. Specifically, the formation and evolution of shear bands are closely related to the deformation strain and the local shear strain.

Obviously, both detwinning and shear bands are kinds of unstable, non-uniform plastic deformation, and frequently appear in multiaxial stress states with large deformation strains and high shear stresses or strains [19, 21, 26]. As such, a quantitative understanding the deformation mechanisms related to detwinning and shear bands of nt-metals under complex stress states and large strain conditions is imperative.

In this work, the microstructure evolution of bulk nt-Cu with preferentially oriented nanotwins subjected to cold rolling with different strains of 15%, 50% and 65% is systematically investigated. Deformation microstructures, such as dislocation morphology, twin thickness distribution, and boundary misorientation have been characterized by electron backscatter diffraction (EBSD) and TEM to reveal the deformation mechanisms of nt-Cu under complex axial deformation. Local shear strains in detwinning regions and shear bands are measured using the TBs as a reference. Our work reveals that the local shear strain plays an important role in the formation of detwinning and shear bands under cold rolling. Eventually, both detwinning and shear bands lead to the evolution of a stable laminated structure.

2. Experimental

High-purity Cu sheets with nanoscale growth twins were synthesized by means of direct-current electrodeposition using an electrolyte of $CuSO_4$. The substrate was a pure Ti sheet. By carefully controlling the deposition parameters, a nt-Cu sheet with preferentially oriented nanoscale twins was deposited to a thickness of ~1.5 mm. More details of the procedure can be found in Ref. [7].

Specimens with an area of 5×3 mm^2 were cut from the as-deposited Cu sheet. Before cold rolling, the specimens were mechanically ground to a final thickness of ~1 mm after mechanical polishing and chemical polishing. Cold rolling was carried out on a twin-roller apparatus with roll diameter of 40 mm at room temperature. During cold rolling, the specimens were placed with the normal direction (ND) of the rolling plane parallel to the growth direction (GD) (figure 1d). As a consequence, both the

rolling direction (RD) and transverse direction (TD) are perpendicular to GD. The rolling strain (ε) is defined as the thickness reduction,

$$\varepsilon = (h_0 - h)/h_0 \quad (1)$$

where h_0 is the initial sample thickness, and h is the final thickness after rolling. The strain rate of the cold rolling is estimated to be $10^{-2} \sim 10^{-1}$ s^{-1}. Three rolling strains of 15%, 50% and 65% were selected to evaluate the microstructure evolution of the cold-rolled nt-Cu.

The microstructures of the as-deposited Cu specimens were examined using a field emission gun scanning electron microscope (SEM) in a FEI Nova NanoSEM 430 with backscattered electron (BSE) imaging using a VCD detector. The electron backscattered diffraction (EBSD) measurements and analysis were performed on the longitudinal section (perpendicular to TD) of the as-rolled samples using the HKL channel 5^{TM} software suite. The step sizes were 200 nm and 50 nm for each sample. Samples for EBSD measurements were first mechanically ground, followed by electro-polishing in a solution of 25% phosphoric acid, 25% alcohol and 50% deionized water at room temperature.

The microstructures of both the as-deposited and the as-rolled nt-Cu samples taken from the longitudinal plane were further characterized using a JEOL 2010 TEM at an accelerating voltage of 200 kV. The TEM foils fixed to 3 mm diameter Cu rings were thinned by twin-jet polishing in an electrolyte of 33% phosphoric acid, 33% alcohol and 33% deionized water at about -10 ℃. This microscope was also equipped with a semi-automatic Kikuchi diffraction analysis technique [33] to allow measurement of the crystallographic orientation of individual crystallites.

3. Results

3.1. Microstructure characteristics of the as-deposited nt-Cu sample

The microstructure of the as-deposited nt-Cu was characterized from both the plane view and the cross-section view. The plane-view SEM image in figure 1a reveals that the as-deposited Cu consists of homogenously distributed equiaxed polycrystalline grains with an average grain size of 3 μm (the grain size distributes from 1 to 6 μm). Most grains are separated by sharp and clear grain boundaries. Only in a portion of grains are straight planar substructures clearly seen.

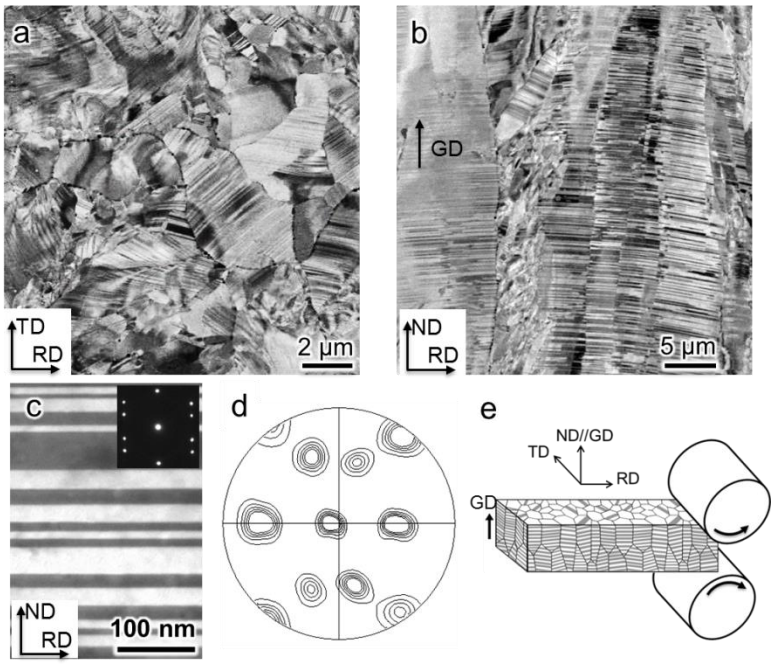

Figure 1. SEM images of the as-deposited columnar nt-Cu sample in plane view (a) and cross-section view (b). GD represents the grown direction of the deposited samples. (c) Cross-sectional TEM observation. The inset shows the corresponding selected area electron diffraction (SAED) pattern. (d) Pole figure taken from plane view data showing a strong <111> out of plane texture. (e) The rolling geometry with respect to the as-deposited specimen. Here ND, TD and RD are the normal direction, transverse direction and rolling direction of the rolled sample, respectively.

Cross-sectional SEM observations (figure 1b) indicate that most grains in the as-deposited Cu are columnar in shape with their longitudinal axis parallel to the GD. Each columnar grain is further

divided by a high density of TBs, which are roughly parallel to the deposition plane. Cross-sectional TEM observation (figure 1c) indicates that the TBs are clear {111} coherent TBs with few dislocations. Analysis of a statistically representative number of edge-on TEM images reveals an average twin thickness (λ) of about 30 nm. The as-deposited sample shows a strong <111> out-of-plane texture in GD, as displayed in the {111} pole figure derived from the EBSD data (figure 1d). A three-dimensional (3D) sketch showing the microstructure of the as deposited Cu is illustrated in figure 1e. The ND during cold rolling is parallel to the GD of the as-deposited nt-Cu sample (ND//GD). As a consequence, the rolling plane (containing RD and TD) is parallel to the TBs.

3.2. Microstructure characteristics of the as-rolled nt-Cu with a rolling strain of 15%

Figure 2 shows the deformation microstructure of nt-Cu sample with a rolling strain of 15%. As displayed in the inverse pole figure (IPF) map colored according to ND (figure 2a), most grains (volume fraction of more than 80%) have a ND close to <111>, which suggests a strong <111> texture in the GD, coinciding with that of the as-deposited nt-Cu. There is no apparent change in the shape of the columnar grains, compared to the as-deposited structure (figure 1b). The grain boundaries are still clear and sharp. Some local shear deformation takes place, however, inside the columnar grains (as indicated by the white arrows in figure 2a), along the direction at ±45 °respective to RD, and resulting in obvious deviation from the original <111> orientation.

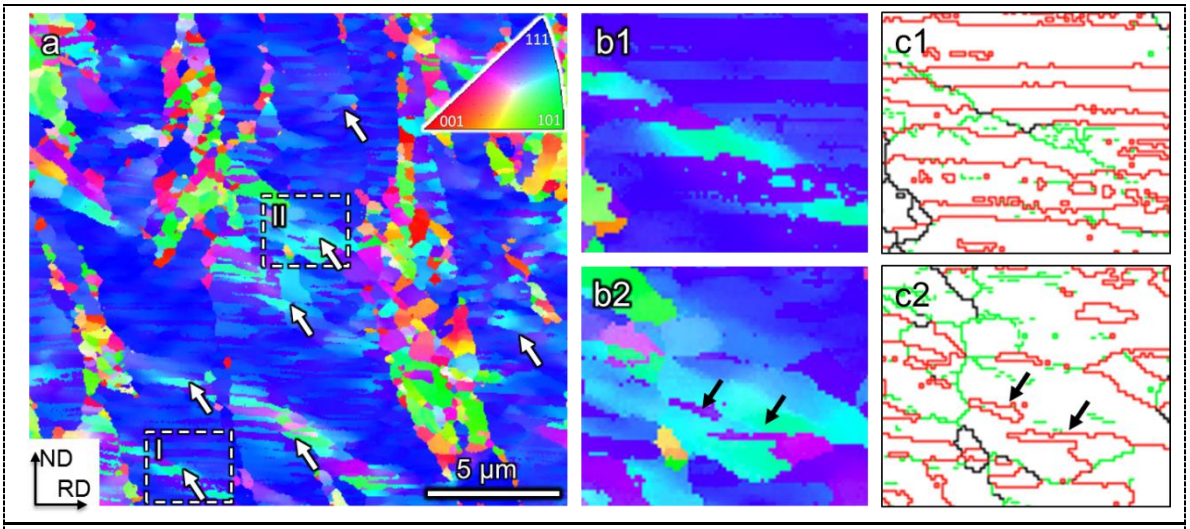

Figure 2. (a) IPF map of cold rolled nt-Cu sample after a strain of 15%, colored according to the ND. Local shear regions are indicated by white arrows. (b1-b2) Enlarged IPF maps of the white squares labeled as "I" and "II" in (a), respectively. (c1-c2) Boundary maps corresponding to (b1-b2). Twin fragments are indicated by black arrows. In the boundary maps, green and black lines represent boundaries with misorientation angles, θ, of $\theta \leq 15°$ and $\theta > 15°$, respectively; red lines represent the Σ3 TBs.

Two sorts of local shear deformation structures with different morphologies can be distinguished in the nt-Cu sample after a rolling strain of 15%. Typical examples for these two deformation structures, white squares I and II, are further revealed by the enlarged IPF maps (figure 2b1 and 2b2) and the boundary maps (figure 2c1 and 2c2). The enlarged IPF map of the local shear region I (figure 2b1) is composed of coarse twin/matrix (T/M) lamellae of more than 100 nm thick, which still have coherent TBs, confirmed by the boundary map in figure 2c1. Low angle grain boundaries with boundary misorientations of 8~10° (measured from figure 2b1) are formed along the edge of this local shear region I (green lines in figure 2c1), leading to deviations from the original <111> direction. This observation suggests extensive slip and accumulation of perfect dislocations in this region.

The local shear region II (figure 2b2) shows a typical morphology of shear bands composed of elongated sub-grains or dislocations cells inclined to the original TBs along ±45 ° direction with

respect to RD. The misorientations of deformed structures in the shear bands is about 8~15° deviation to the original <111> orientation. The corresponding boundary map (figure 2c2) indicates that most sub-grains in the shear band are associated with low angle dislocation boundaries. The narrow sub-grains surrounded by TBs (black arrows in figure 2b2 and 2c2) in the shear bands are preserved twin lamellae fragments. Clearly, the formation of shear bands destroys the original twin lamellae, and then dislocation cells and boundaries are formed along the shear direction.

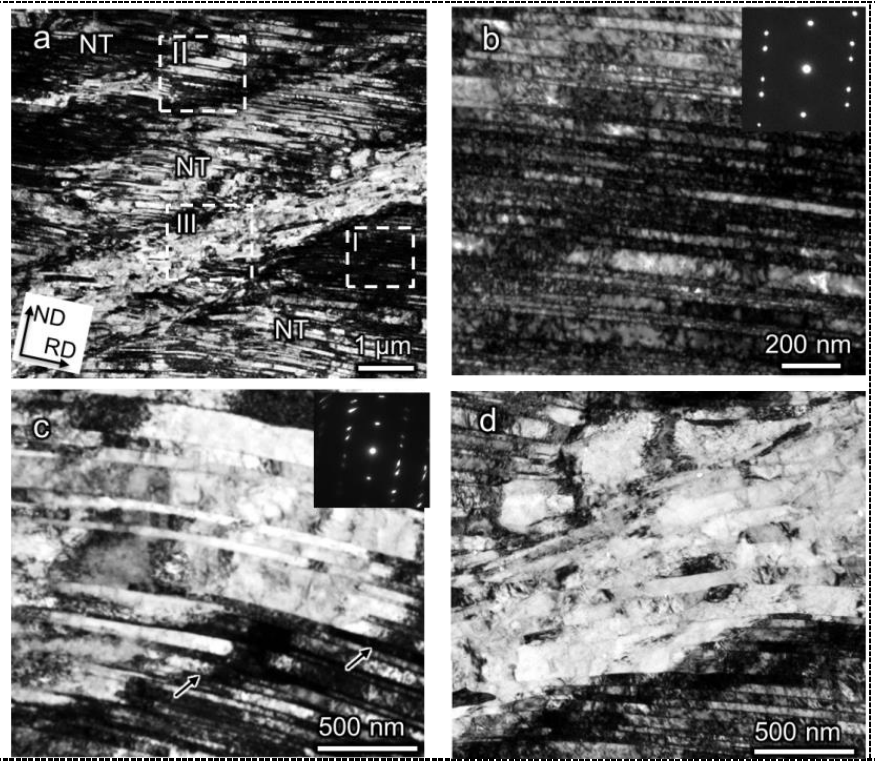

Figure 3. (a) TEM image of cold rolled nt-Cu sample after a strain of 15%. (b-d) High magnification images of the corresponding regions labeled as "I", "II" and "III" in (b), showing the nanoscale twin structure, the coarse twin structure and a shear band in detail, respectively. The insets in (b) and (c) are the corresponding SAED patterns of the nanotwins and the coarse twin structure. The interface between the detwinning region and preserved nanotwins is indicated by black arrows in (c).

More detailed TEM observations were carried out to characterize the detailed microstructure of nt-Cu samples after a rolling strain of 15%. The low magnification TEM observation of the nt-Cu in figure 3a shows the appearance of a few parallel locally sheared regions along a direction about 35° with respect to RD, cutting through the original nanoscale twin lamellae (marked by "NT"). Three typical microstructures are selected for further detailed analysis, namely preserved nanoscale twin structure, coarse T/M lamellae, and shear band, as indicated by the white squares "I", "II" and "III", respectively. An enlarged image of the preserved nanoscale T/M lamellae in white square "I" (figure 3a) shows that the TBs are well preserved, with a strict T/M relationship, as detected by SAED. A high density of dislocations appears inside each T/M lamellae and is accumulated at the TBs, which indicates that the plastic deformation in this region is mainly carried by extensive activity of perfect dislocations.

In comparison with the well preserved fine twin lamellae, in a local detwinning (region "II" , figure 3c), most of the fine twin lamellae of width less than 100 nm are annihilated and only coarse lamellae with lamellar thicknesses of 100 nm ~200 nm are detected. The SAED pattern (the inset in figure 3c) indicates that the coarse lamellae are still separated by TBs but that the zone axis deviates slightly from the [011] axis of the well preserved nanoscale twins (see inset in figure 3b). A high density of dislocations are accumulated at the interface between the detwinning region and the preserved nanoscale twins, lead to an obvious misorientation (arrows in figure 3c).

In contrast to the detwinning region (figure 3c), much more severe deformation takes place in the shear band, as shown in figure 3d (white square "III" in figure 3a), where the nanoscale twins are completely destroyed. Elongated sub-grains or dislocation cells are formed inside the shear band and lie along the direction of the shear bands, which are inclined to the preserved TBs.

To quantify the local plastic deformation associated with a given shear band or detwinning region, local shear strains in detwinning and shear bands are measured by using the curved TBs as markers [32]. Figure 4a and 4b are typical TEM images of a detwinning region and a shear band of 15% cold rolled Cu sample, in which the preserved TBs (red dotted lines in figure 4a and 4b) are used as a reference to calculate the local shear strains. A fiducial line is drawn following the TB and is divided into a series of segments of equal width, ***d***, in the direction perpendicular to the shear banding direction (figure 4c). The average shear strain associated with each segment is then calculated according to:

$$\gamma = d/\delta = ctg\theta - ctg\theta_0, \quad (2)$$

where the parameters d, δ, θ, θ_0 are defined as shown in figure 4c. θ_0 is the angle of the shear direction (AA') to the direction of the original TB (BB'); θ is the angle of the shear direction (AA') to the direction of curved the TB (CC'); δ is the width (transverse to the shear direction) of a unit segment, and d is the shear displacement of a unit segment.

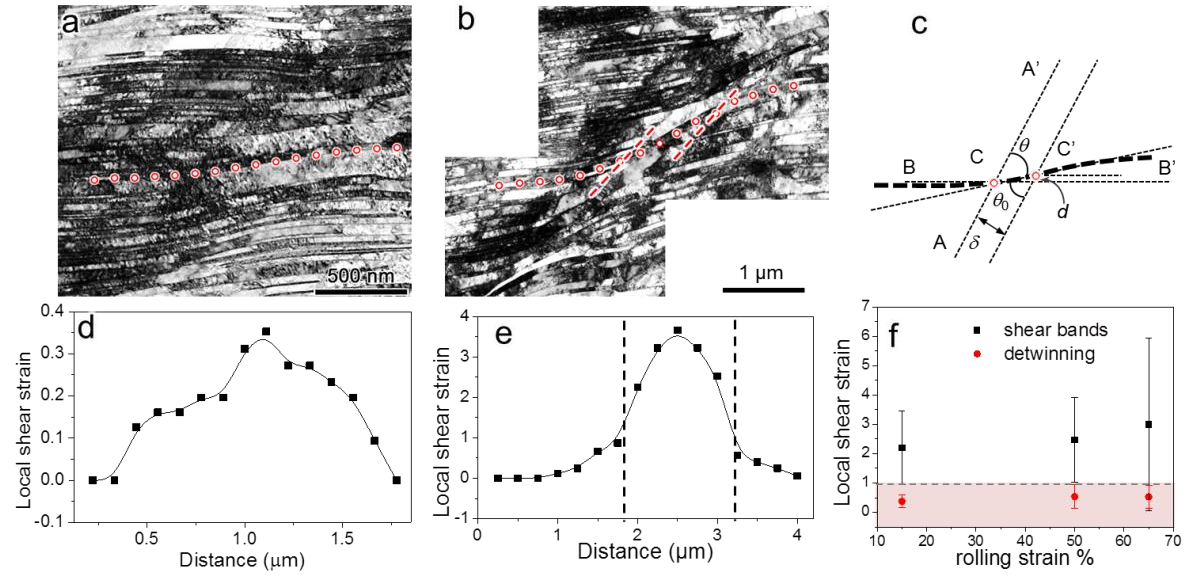

Figure 4. TEM images of a detwinning region (a) and a shear band (b). (c) Geometric relation for calculating the shear strain. θ_0 is the angle of the shear direction (AA') to the direction of the original TB (BB'); θ is the angle of the shear direction (AA') to the direction of the curved TB (CC'); δ is the width (transverse to the shear direction) of a unit segment; d is the shear displacement of a unit segment. (d) and (e) Distributions of shear strain along the TB marked by dashed lines in (a) and (b), respectively. (f) Local shear strains of shear bands and detwinning regions at different rolling strains.

Figures 4d and 4e indicate the distribution of the local shear strains in the detwinning region and the shear band, respectively. A single saddle-shape distribution of the local shear strains is observed in both the detwinning region and in the shear bands, i.e., the local shear strains rise up from almost zero on the edge to a peak in the core. The maximum shear strain in the center of the detwinning region approaches γ_{max} = 0.4 (figure 4d), whereas this value can be as large as 3.6 for the shear band (figure 4e).

Statistic results of local shear strains measurements in the detwinning region and in shear bands in the nt-Cu samples under different strains are summarized in figure 4f. It is found that the local shear strains in detwinning regions are less than 1, and are insensitive to the rolling strain. In contrast, in the shear bands, the local shear strains are larger than 1 and increase slightly with increasing rolling strain. This means that it is the local shear strain, rather than the nominal rolling strain that induces detwinning or the formation of shear bands during cold rolling of nt-Cu.

Based on the above SEM and TEM observations, it is found that both homogeneous and inhomogeneous deformations are observed in nt-Cu after a rolling strain of 15%. More than 80% of the nanotwins are preserved. Local shear deformation microstructures including detwinning and shear bands are already present at this strain level.

3.3. Microstructure characteristics of the as-rolled nt-Cu with a rolling strain of 50%

As the rolling strain is increased to 50%, non-uniform deformation is prevalent in the nt-Cu. As shown in the IPF map (figure 5a), a large amount of detwinning (white arrows) and shear bands (black arrows) form along ±45° to RD, which can be easily recognized by orientations deviated from the original <111> direction. As a result, the deformation structure presents a net-like morphology, where the original columnar grains are hard to identify. Nanoscaled twins with the original <111> orientation are cut into blocks (labeled as "NT"). The volume fraction of preserved nanoscaled twins is reduced to less than 30%. Compared to the nt-Cu sample after a rolling strain of 15%, shear bands run across many grains, and are wider and longer, and tend to lie parallel to RD direction. Moreover, the orientations within shear bands deviate 20-25° from the original <111> orientation, a much larger deviation than that in 15% cold rolled samples.

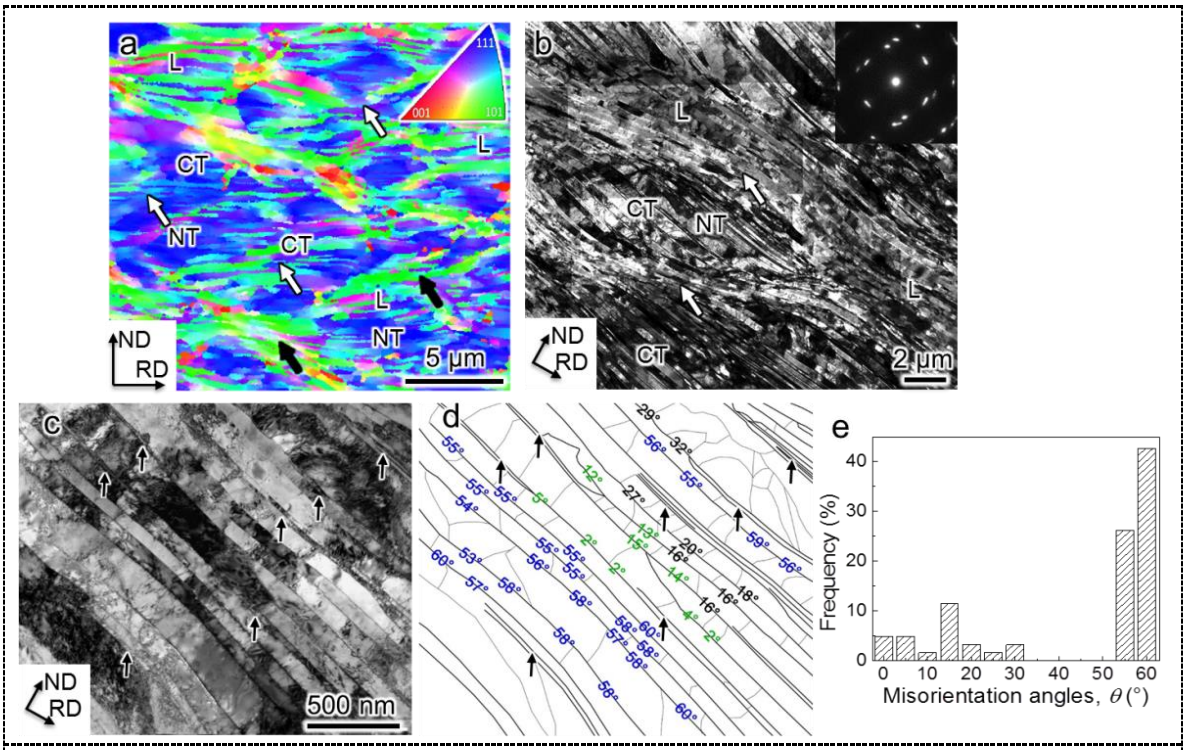

Figure 5. IPF map (a) and TEM image (b) of cold rolled nt-Cu sample after a strain of 50%. The inset in (b) shows the corresponding SAED pattern of the NT bundle. Nanoscaled twins, coarse T/M lamellae and laminated structure are labeled as "NT", "CT" and "L", respectively. The detwinning regions and shear bands are indicated by white and black arrows, respectively. (c) High magnification TEM image of the laminated structure. (d) Sketch corresponding to (c), where misorientation angles are marked across the lamellar boundaries. Fine twin lamellae fragments are indicated by black arrows in (c) and (d). (e) Misorientation angle distribution of the lamellar boundaries.

As shown in figure 5a, a large amount of coarse twins (CT), with a volume fraction of ~50%, are formed by extensive detwinning. The orientations of the detwinning regions are deviated by 10-12° from the original <111> orientation, which is almost the same as for the detwinning regions in the 15% rolled samples. In addition, a kind of newly formed laminated structure ("L"), with similar morphology and comparable lamellar thicknesses to that of the coarse T/M lamellae but without any

T/M relationship, is observed. The orientations in laminated structure deviate 20-25° from the original <111> orientation, larger than that of the coarse twin regions.

The TEM image of nt-Cu after a rolling strain of 50% in figure 5b indicates typical laminated structures along RD, with some preserved twin blocks, including nanoscale twins and coarse T/M lamellae surrounded by shear bands. The SAED pattern shows that some lamellar boundaries are no longer TBs but high angle boundaries (HABs). Sub-grains in shear bands are stretched and curved along the edge of twin blocks, presenting an elongated morphology similar to the laminated structures but finer.

The higher magnification image of the laminated structures in figure 5c reveals that the extended lamellar boundaries are sharp and flat with thicknesses of more than 100 nm. Numerous dislocations are present inside the lamellar channels, forming dislocation cells and interconnecting boundaries. The misorientation angles across the lamellar boundaries analyzed by Kikuchi diffraction (figure 5d) show a representative character of very high angle misorientations (larger than 50°) across the laminated boundaries. This is much higher than for lamellar boundaries produced by cold rolling of conventional coarse grained metals, but close to 60° for a coherent TB. A few fine twin lamellae fragments with twin thickness less than 50 nm (black arrows) can be observed. Two fragments of fine twin lamellae are connected by low angle boundaries (LABs), indicating the annihilation of fine twin lamellae. Extensive statistical analysis (figure 5e) indicates that the laminated structures are composed ~80% of HABs with more than 50° misorientation, and ~10% of LABs. The above observations suggest that these laminated structures are evolved from coarse T/M lamellae formed by detwinning.

Clearly, when the nt-Cu sample is rolled to a strain of 50%, detwinning and shear bands are extensively activated, cutting the original nanoscale twins into blocks. As a result a typical laminated structure, separated by HABs of more than 50°, begins to form.

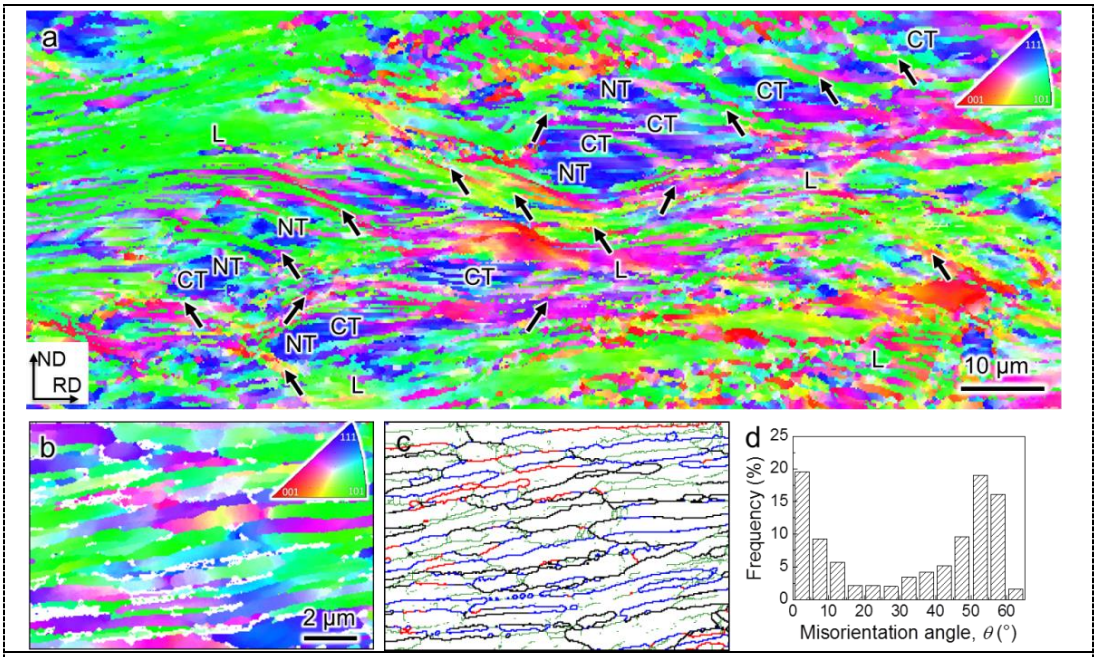

Figure 6. (a) IPF map of cold rolled nt-Cu after a strain of 65%. Shear bands are indicated by black arrows. (b) High magnification IPF map of the laminated structure. Shear bands are indicated by black arrows. (c) Boundary map corresponding to (b). In the boundary maps, green and black lines represent boundaries with misorientation angles θ, $\theta \leq 15°$, and $\theta > 15°$, respectively; red lines represent the $\Sigma 3$ TBs. (d) Misorientation angle distribution of the lamellar boundaries. The nanoscaled twins, coarse T/M lamellae and laminated structures are labeled as "NT", "CT' and "L", respectively.

3.4. Microstructure characteristics of the as-rolled nt-Cu with a rolling strain of 65%

As shown in the IPF map (figure 6a), as the rolling strain increases to 65%, the microstructure presents a wavy lamellar morphology. Most of the original nanoscale twins are replaced by laminated structures ("L") with a volume fraction of more than 70%. The original nanoscale twins are cut into twin blocks including most of the coarse T/M lamellae ("CT") and very few preserved nanoscale twins ("NT") by shear bands (black arrows in figure 6a) and laminated structures. The coarse T/M lamellae ("CT") deviate by 8-12 °from the original <111> direction, whereas the nanoscale twins still maintain their original <111> direction. Sub-grains in the shear bands are further elongated and rotate, then evolve into laminated structures, slightly inclined to the RD.

A high magnification IPF map (figure 6b) and corresponding grain boundary map (figure 6c) reveal that the laminated structures are separated by longitudinal boundaries composed of many HABs of angle in the range $50°<\theta<60°$ (blue lines in figure 6c), a few Σ3 coherent TBs (red lines in figure 6c) and few LABs of angle $\theta<15°$ (green lines along RD in figure 6c) roughly parallel to RD. As a result, a statistical analysis of boundary misorientations (figure 6d) shows a bimodal distribution with peaks at 5° and 55°. Here the HABs corresponding to the peak at 55° come from the longitudinal boundaries evolving from the TBs, in accordance with the observations on the 50% rolled sample. The large number of LABs should, however, be attributed to dislocations cells and boundaries formed inside the lamellae (short green lines in figure 6c).

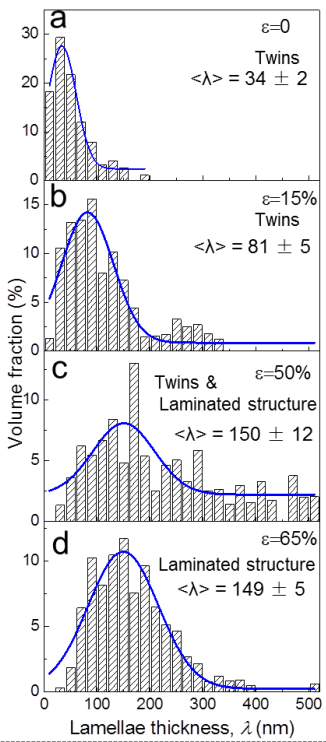

Figure 7. Lamellae thickness distributions of as deposited (a) and cold rolled nt-Cu samples at different strains of 15% (b) , 50% (c) and 65% (d).

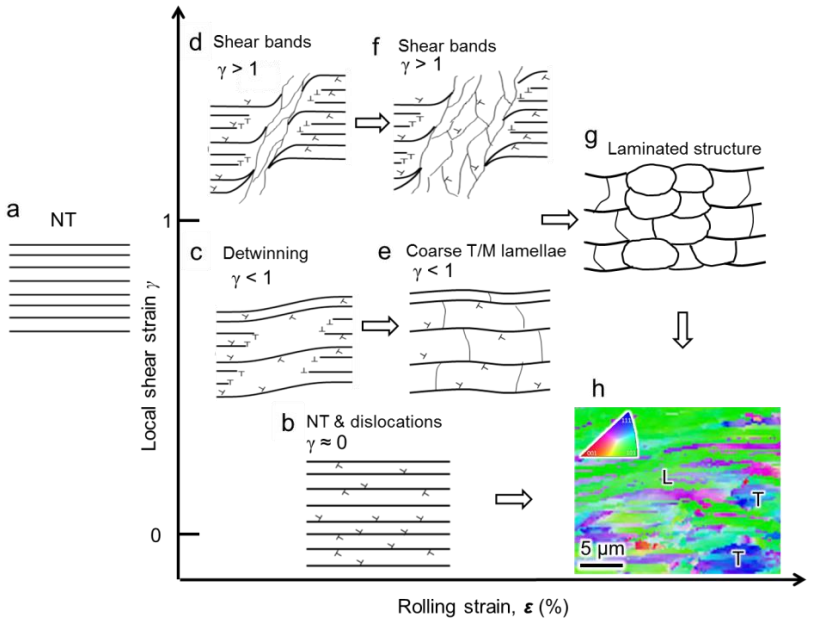

Figure 8. Schematic illustration of the deformation structure evolution during cold rolling of nt-Cu. The twin blocks and laminated structures are labeled as "T" and "L", respectively.

The distribution of lamellae thickness values for the laminated structure, as measured from TEM data in samples at different rolling strains is shown in figure 7. When detwinning begins to happen at 15% rolling strain, coarse T/M lamellae with an average thickness of ~80 nm and a wide distribution extending to more than 300 nm are formed. After universal detwinning, the average thickness of coarse T/M lamellae reaches 150 nm (figure 7c). The average lamellar thicknesses of the laminated

structure, as well as of the coarse T/M lamellae, reaches a saturated value about 150 nm (figure 7c and 7d) during microstructure evolution to larger rolling strains. This also strongly supports the idea that the laminated structure evolves from the coarse T/M lamellae. It should be noted that this saturated lamellar thickness of the as-rolled nt-Cu is finer than that of lamellar boundaries (230 nm) formed in conventional coarse Cu cold rolled to a sufficiently high strain [34].

For the sample rolled to a strain of 65% the results show that a laminated structure containing HABs with misorientation angles of more than 50° and average thicknesses of ~150 nm embedded with a few preserved twin blocks are eventually formed.

4. Discussion

The structural evolution and deformation mechanism of polycrystalline metals have been well studied and reported in the literature [34-40]. It has been found that the microstructure evolution is one of continuous subdivision by dislocation boundaries, including incidental dislocation boundaries (IDBs) and geometrically necessary boundaries (GNBs), arising from the extensive forest dislocation activity with increasing strain [35-37]. The boundary alignment is inclined to the rolling direction at low strains in a manner closely related to the grain orientation [35]. At a strain of about 65% and above, this structure evolves into a saturated structure of lamellar dislocation boundaries almost parallel to the rolling plane [34, 35]. With increasing cold rolling strain, the boundary spacing decreases and can reach 50–300 nm, as exemplified in cold rolled Al, Ni, Cu and Fe [38-40]. At the same time, the misorientation angle across the boundaries increases substantially and reaches a saturated average value of 40° as the dislocation boundaries finally develop into HABs.

Different from plastic deformation mechanisms dominated by the interactions of forest dislocations in coarse grained face-centered cubic metals, the plastic deformation of nt-Cu is dominated by interactions between dislocations and TBs [7, 19]. The stress state of nt-Cu in this rolling deformation can be assumed as a combination of both compression in the ND (perpendicular to the TBs) and tension in the RD (parallel to the TBs). The uniform deformation will be accommodated by perfect dislocations transmitting across, and piling up at, the TBs or threading inside the T/M lamellae [41]. The uniform plastic strain is, however, very limited (~1%) for nt-Cu with fine grain sizes of less than 3 μm [3]. Both of these two kinds of dislocation behavior are heavily suppressed by the TBs with an average spacing in the nanoscale. Meanwhile, partial dislocations slipping along the TBs can hardly be activeted, due to the limited shear stress on the TBs. Consequently, the uniform deformation of nt-Cu is limited, and strain localization takes place ±45° with respect to the RD direction, where there is an obvious stress concentration during cold rolling.

Strain localization leads to numerous perfect dislocations transmitting and interacting with TBs by dislocation reactions, producing many Shockley partials [19, 41]. Both transmission of perfect dislocations, or pile ups on TBs and partial dislocations gliding along the TBs sustain the local shear strains. The motion of Shockley partials on the TBs leads to detwinning of fine twin lamellae, similar to the detwinning process observed in in-situ TEM experiments [19]. Detwinning contributes a shear strain of $\boldsymbol{b}\langle 112\rangle/d\{111\}=0.707$ along the detwinning direction [42], which has a component of $0.707\cos\theta$ (figure 6c) along the shearing direction (inclined to the TBs). Combined with the contribution of perfect dislocations, the maximum local shear strain taken by detwinning reaches a value of about 1, as illustrated in the former observation.

After detwinning, further rolling strain is taken by the activity and interaction of perfect dislocations from different slip systems, instead of the activity of a dominant single slip system in the nanoscaled twins. Dislocations continuously accumulate on the TBs, breaking the T/B relationship. The coarse T/M lamellae finally evolve into a laminated structure with HABs of more than 50° misorientation angle and a comparable lamellar thickness to the coarse T/M lamellae. The HABs of the laminated structure originate from the initial TBs, in contrast to HABs formed in cold rolled coarse-grained metals, which instead originate from dislocation boundaries with increasing boundary misorientations as the rolling strain increases [40].

In the region with severe local shear strains (>1), accumulation of perfect dislocations and transmission across TBs dramatically happens under higher stress concentrations, leading to the

destruction of the fine twins. The local shear strains are taken by continuous slip and interaction of perfect dislocations. As a result, shear bands containing dislocation cells, and sub-grains as well as a few broken twin lamellae are formed. Upon further rolling, the shear bands grow longer and wider under a high local shear strain. Further deformation in these shear bands is taken by the activation and interaction of dislocations. The dislocation cells, sub-grains and fragments of twin lamellae inside the shear bands eventually evolve into laminated structures, which are slightly inclined to RD. Similar to laminated structures evolving from coarse T/M lamellar, the laminated structures from shear bands are also composed of HABs resulting from the twin boundaries and of LABs coming from dislocation cells.

The evolution of the deformation microstructure of nt-Cu (figure 8a) under cold rolling is summarized in figure 8. At a very small rolling strains, uniform deformation assisted by dislocation slip inside the nanoscale twins and accumulation at TBs (figure 8b) dominates the plastic defamation. Strain localization takes place in some grains, taken by detwinnning (figure 8c) and shear bands (figure 8d), closely related to the local shear strain with a critical value about 1, regardless of local crystal orientation. Detwinning is substantially promoted in the grains with local shear strains <1, produced extensive coarse T/M lamellae (figure 8e). Additionally, the shear bands grow wider and longer (figure 8f) under a large local shear strain (>1). With further increase of rolling strain, strain localization intensifies. Finally, both the coarse T/M lamellae and the shear bands evolve into a saturated laminated structure containing HABs (misorientation angle larger than 50°) (figure 8g). The eventual deformation structure of the nanotwinned Cu sample under cold rolling consist of the massive laminated structures embedded with a few blocks of preserved twins (figure 8h).

5. Conclusions

We have systematically studied the microstructure evolution of highly-oriented nt Cu samples under cold rolling to strains of 15%, 50% and 65%. At a rolling strain of 15%, uniform deformation, carried by the interactions between dislocations and twin boundaries, dominates. At the same time, a small amount of strain localization, carried by detwinning and shear bands in a direction 45 ° respective to the rolling direction, take place. As the rolling strain is increased to 50%, detwinning becomes a dominant deformation mechanism and produces a large amount of coarse twin structure. As the rolling strain is further increased up to 65%, an extensive stable laminated structure, embedded with a few preserved twin blocks, is formed.

It is found that the local shear strain plays a critical role in the microstructure evolution of the nanotwinned Cu under cold rolling. When the local shear strains are so small as to be negligible, uniform deformation is accommodated by the interactions of dislocations with twin boundaries, and the nanoscale twins survive. As the local shear strains reach up to 1 (<1), detwinning prevails and results in coarse twin/matrix lamellae. When the local shear strain is larger than 1, the formation of shear bands, composed of dislocation cells, sub-grains and fragments of twin lamellae, takes place instead of detwinning, eventually evolving to produce an extensive laminated structure.

This study sheds lights on the understanding on the deformation physics of nt-metals under complex stress states and large strain, in particular regarding the heterogeneous deformation behavior including detwinning and formation of shear bands in nt-metals.

Acknowledgments

L. Lu acknowledges the financial support by the National Science Foundation of China (Grant Nos. 51471172, 51420105001 and U1608257) and the Key Research Program of Frontier Science, CAS. We thank Mr. S. Jin for his assistance in sample preparation.

6. References

[1] Lu L, Shen YF, Chen XH, Qian LH, Lu K 2004 *Science*, **304** 422-26.
[2] Zhang X, Wang H, Chen XH, Lu L, Lu K, Hoagland RG, Misra A 2006 *Appl. Phys. Lett.*, **88** 173116.
[3] You ZS, Lu L, Lu K 2011 *Acta Mater.*, **59** 6927-37.
[4] Pan Q, Zhou H, Lu Q, Gao H, Lu L 2017 *Nature*, **551** 214-17.

[5] Lu L, Chen X, Huang X, Lu K 2009 *Science*, **323** 607-10.
[6] Hodge AM, Wang YM, Barbee TW Jr 2008 *Scr. Mater.*, **59** 163-66.
[7] You ZS, Li XY, Gui L J, Lu QH, Zhu T, Gao HJ, Lu L 2013 *Acta Mater.*, **61** 217-27.
[8] Lu Q, You Z, Huang X, Hansen N, Lu L 2017 *Acta Mater.*, **127** 85-97.
[9] Dao M, Lu L, Shen YF, Suresh S 2006 *Acta Mater.*, **54** 5421-32.
[10] Li X, Wei Y, Lu L, Lu K, Gao H 2010 *Nature*, **464** 877-80.
[11] Jin ZH, Gumbsch P, Albe K, Ma E, Lu K, Gleiter H, Hahn H 2008 *Acta Mater.*, **56** 1126-35.
[12] Jin ZH, Gumbsch P, Ma E, Albe K, Lu K, Hahn H, Gleiter H 2006 *Scr. Mater.*, **54** 1163-68.
[13] Chen XH, Lu L, Lu K 2011 *Scr. Mater.*, **64** 311-14.
[14] Shen YF, Lu L, Lu QH, Jin ZH, Lu K 2005 *Scr. Mater.*, **52** 989-94.
[15] Jia D, Ramesh K T, Ma E, Lu L, Lu K 2001 *Scr. Mater.*, **45** 613-20.
[16] Shen YF, Lu L, Dao M, Suresh S 2006 *Scr. Mater.*, **55** 319-22.
[17] Wang HT, Tao N R, Lu K 2012 *Acta Mater.*, **60** 4027-40.
[18] Zhang X, Misra A, Wang H, Nastasi M, Embury JD, Mitchell TE, Hoagland RG, Hirth J P 2004 *Appl. Phys. Lett.*, **84** 1096-98.
[19] Wang J, Li N, Anderoglu O, Zhang X, Misra A, Huang JY, Hirth JP 2010 *Acta Mater.*, **58** 2262-70.
[20] Lu QH, Sui ML, Huang XX, Li DX, Hansen N 2014 *Philos. Mag.*, **94** 2262-80.
[21] Hodge AM, Furnish TA, Shute CJ, Liao Y, Huang X, Hong CS, Zhu YT, Barbee T W, Weertman J R 2012 *Scr. Mater.* **66** 872-77.
[22] Liu Y, Jian J, Chen Y, Wang H, Zhang X 2014 *Appl. Phys. Lett.*, **104** 231910.
[23] Cao Y, Wang YB, Chen ZB, Liao XZ, Kawasaki M, Ringer SP, Langdon TG, Zhu YT 2013 *Mater. Sci. Eng. A*, **578** 110-14.
[24] Lee S, Im J, Yoo Y, Bitzek E, Kiener D, Richter G, Kim B, Oh SH 2014 *Nat. Commun.*, **5** 3033.
[25] Cheng G, Yin S, Chang TH, Richter G, Gao H, Zhu Y 2017 *Phys. Rev. Lett.*, **119** 256101.
[26] Hong CS, Tao NR, Huang X, Lu K 2010 *Acta Mater.*, **58** 3103-16.
[27] Wang J, Misra A, Hirth JP 2011 *Phys. Rev. B*, **83** 064106.
[28] Li N, Wang J, Zhang X, Misra A 2011 *JOM*, **63** 62.
[29] Hodge AM, Furnish TA, Navid AA, Barbee TW Jr. 2011 *Scr. Mater.*, **65** 1006-09.
[30] Duggan BJ, Hatherly M, Hutchinson WB, Wakefield PT 1978 *Met. Sci.*, **12** 343-51.
[31] Xiao GH, Tao NR, Lu K 2009 *Mater. Sci. Eng. A*, **513-514** 13-21.
[32] Hong CS, Tao NR, Huang X, Lu K 2010 *Acta Mater.*, **58** 3103-16.
[33] Liu Q 1994 *J. Appl. Crystallogr.*, **27** 755-61.
[34] Takata N, Yamada K, Ikeda K-i, Yoshida F, Nakashima H, Tsuji N 2007 *Mater. Trans.*, **48** 2043-48.
[35] Huang X, Winther G 2007 *Philos. Mag.*, **87** 5189-14.
[36] Winther G, Huang X 2007 *Philos. Mag.*, **87** 5215-35.
[37] Bay B, Hansen N, Hughes DA, Kuhlmannwilsdorf D 1992 *Acta Metall. Mater.*, **40** 205-19.
[38] Liu Q, Huang X, Lloyd DJ, Hansen N 2002 *Acta Mater.*, **50** 3789-02.
[39] Malin AS, Hatherly M 1979 *Met. Sci.*, **13** 463-72.
[40] Hughes DA, Hansen N 2000 *Acta Mater.*, **48** 2985-3004.
[41] Zhu YT, Wu XL, Liao XZ, Narayan J, Kecskes LJ, Mathaudhu SN 2011 *Acta Mater*, **59** 812-21.
[42] De Cooman BC, Estrin Y, Kim SK 2018 *Acta Mater.*, **142** 283-362.